A study of the growth mechanism of large-diameter double-wall TiO$_2$ nanotube arrays fabricated by high voltage anodization

Chunhai Ke[1], Jingyun Ma[1], Jiahua Ni[2], Zhaoxiang Peng[1]

[1]Ningbo Medical Center, Lihuili Hospital, Ningbo University, Ningbo, China; [2]Ningbo Regen Biotech, Co., Ltd., Ningbo, China

Contributions: (I) Conception and design: Z Peng, C Ke; (II) Administrative support: J Ni; (III) Provision of study materials or patients: Z Peng, C Ke; (IV) Collection and assembly of data: C Ke, J Ma; (V) Data analysis and interpretation: J Ni; (VI) Manuscript writing: All authors; (VII) Final approval of manuscript: All authors.

Correspondence to: Zhaoxiang Peng. Ningbo Medical Center, Lihuili Hospital, Ningbo University, 57 Xingning Road, Ningbo 315040, China. Email: pzxao@hotmail.com; Jiahua Ni. Ningbo Regen Biotech, Co., Ltd., 168 East Hexiao Road, Ningbo 315100, China. Email: jhni2022@163.com.

Background: Research on the growth mechanism of titanium dioxide (TiO$_2$) nanotube arrays fabricated by anodic oxidation is essential to achieve artificial control of the microstructure and to expand their applications. In our previous work, we reported the preparation of highly ordered large-diameter double-wall TiO$_2$ nanotube arrays prepared by high voltage anodization.

Methods: In this paper, we observed and analyzed the initial growth process of large-diameter double-wall TiO$_2$ nanotube arrays anodized at 120 V in ethylene glycol electrolyte containing aluminum fluoride (NH$_4$F) and water (H$_2$O), such as the evolution of surface and cross-sectional morphologies, the influence of current density on growth rate, the transition process from nanoholes to nanotubes, and the evolution of dimples on the remaining substrate.

Results: On the basis of our observations and inspirations from the existing viewpoints, we established growth models of large-diameter double-wall TiO$_2$ nanotube arrays corresponding to different growth stages to explain the growth process. The growth rate of anodic oxide film changes accordingly with the current density. The compact anodic oxide film formed initially actually contains outer layer and inner layer, with no obvious interface between them. Then, the bottom even levels of the inner layer and outer layer bulge towards the substrate and become individual hemisphere-like structures. The inner layer becomes the outer wall, and the outer layer becomes inner wall. Eventually, V-shaped large-diameter and double-wall TiO$_2$ nanotube arrays form.

Conclusions: The results presented in this work are significant and provide a better understanding of the growth mechanism of large-diameter double-wall TiO$_2$ nanotube arrays anodized by high voltage.

Keywords: TiO$_2$ nanotube arrays; large diameter; double-wall; growth mechanism; high voltage anodization

Introduction

At present, the common methods for preparing titanium dioxide (TiO$_2$) nanotube arrays include hydrothermal method (1), template method (2) and anodic oxidation method (3). Among them, TiO$_2$ nanotube arrays prepared by anodic oxidation method are favored because of the easy morphology control and strong binding with substrate (4,5).

The self-organized TiO$_2$ nanotube arrays fabricated by anodization are extensively useful in various applications, such as drug delivery systems (6,7), orthopedic implants (8,9), dye-sensitized solar cells (10,11), photocatalysis (12,13), and so on (14-16), due to their special surface topologies, superior physical and chemical properties, and excellent biocompatibility, among other qualities (17,18). It is of paramount importance to study the growth mechanism

of TiO_2 nanotube arrays fabricated by anodization to achieve artificial control of microstructure and expand their applications. Understanding of the growth mechanism of TiO_2 nanotube arrays has been largely built upon that of the highly ordered Al_2O_3 nanotube arrays by anodization, which has been investigated extensively (19-22). Zwilling et al. (23) reported that the existence of F^- in electrolyte was necessary for the formation of nanotubular structure. Beranek et al. (24) showed that the growth and dissolution of the TiO_2 nanotube films finally reached a dynamic balance. Mor et al. (25) suggested that the chemical dissolution and field-assisted dissolution were the critical factors for the formation of TiO_2 nanotube during anodization, based on the point defect model proposed by Macdonald (21). Many researchers have asserted that the field-assisted dissolution is the leading mechanism for the information of porous anodization films on valve metals (19,26,27). Skeldon et al. and Garcia-Vergara et al. (28,29) proposed the plastic flow mechanism for growth of porous Al_2O_3 nanohole arrays by anodization, and Houser et al. and Hebert et al. (22,30) established a model of plastic flow mechanism. Roy et al. suggested that the flow mechanism was also applicable to the growth of anodic TiO_2 nanotube arrays (18), and confirmed that a fluoride-rich layer existed at the compact TiO_2 oxide/Ti substrate interface due to the migration of ions through the anodic oxide films (31). Raja et al. (32) reported that the repulsive force originating from cation vacancies was the cause of division of common walls of nanoholes into nanotube wall. Roy et al. (18) proposed that

selective dissolution of fluoride-rich layers and preferential etching at triple points by water (H_2O) in electrolyte resulted in the formation of a tubular structure from an originally porous structure. Although many results for the growth mechanism of anodization TiO_2 nanotube have been yielded, a comprehensive full understanding still does not exist, and the growth mechanism of highly ordered self-organization TiO_2 nanotube arrays prepared by anodization requires further study. Especially for double-wall TiO_2 nanotube arrays, of which the structure and formation conditions are different from single-wall TiO_2 nanotubes (31,33,34), few reports regarding their growth mechanisms are available in the literature.

In the present work, we investigated the initial growth process of the large-diameter double-wall TiO_2 nanotube arrays anodized at high voltage (120 V) in ethylene glycol electrolyte consisting of aluminum fluoride (NH_4F) and H_2O on high purity titanium (Ti) foils at room temperature. The evolution of surface and cross-section morphologies and the transition process from nanoholes to nanotubes were reported in detail. Based on our observations and insights stimulated by some existing viewpoints, we established growth models of large-diameter double-wall TiO_2 nanotube arrays obtained at high voltage in order to better understand their formation. We present the following article in accordance with the MDAR reporting checklist (available at https://atm.amegroups.com/article/view/10.21037/atm-22-6510/rc).

Methods

Materials

Anodization was conducted in a 2-electrode configuration using DC power supplies (GPR-30H10D, GwINSTEK/CE0200010T, Kalaifei, Shanghai, China). The electrolyte consisted of 0.5 wt % NH_4F (96%, Alfa Aesar, Tweksbury, MA, USA) and 10 vol % H_2O in ethylene glycol (99.8%, JT Baker, Mumbai, MH, India), and electrolyte that had been used for ~80–100 hours was used in this paper.

Experiment

The reason for utilizing the used electrolyte was explained in our previous work (33). Titanium sheets (99.5% purity, annealed, 0.25 mm thick, Alfa Aesar) were cut into 12 mm × 24 mm size to serve as the anode electrode. Prior to anodization, samples were degreased in acetone with


Highlight box

Key findings
- We established growth models of large-diameter double-wall TiO_2 nanotube arrays corresponding to different growth stages to explain the growth process.

What is known and what is new?
- There have been many results on the growth mechanism of anodized TiO_2 nanotubes.
- We propose a comprehensive and adequate understanding of the growth mechanism of highly ordered self-organized TiO_2 nanotube arrays prepared by anodic oxidation.

What is the implication, and what should change now?
- This work reveals the growth mechanism of large-diameter double-walled TiO_2 nanotube arrays after high-voltage anodic oxidation, guiding the preparation conditions of this class of materials to adjust to application requirements.
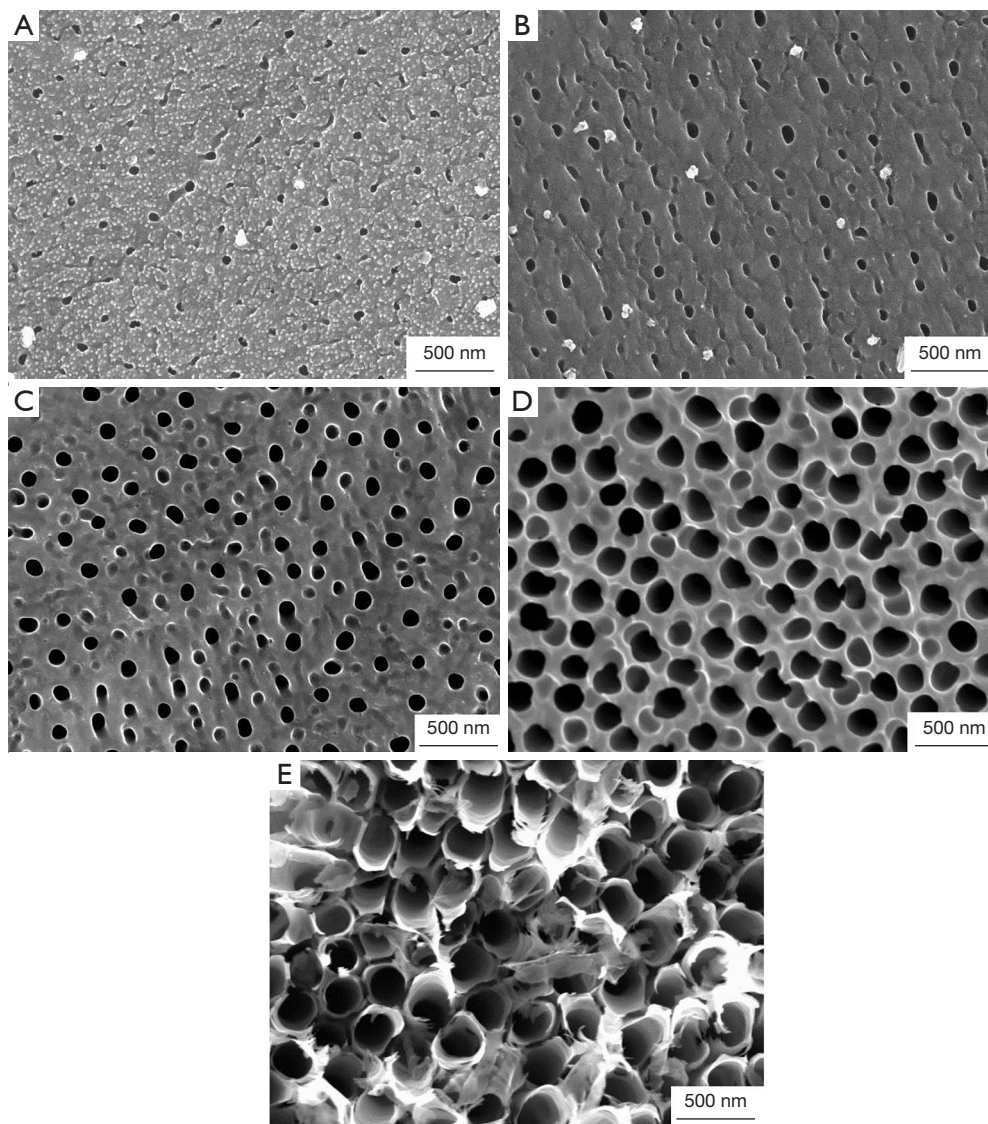
Figure 1 Evolution of surface morphology of Ti anodic oxide films obtained at different oxide times under the voltage of 120 V. (A-E) Anodization for 5 seconds, 15 seconds, 2 minutes, 10 minutes and 20 minutes, respectively.

ultrasonication followed by distilled water rinse, and then chemically etched for 40–60 seconds in the mixture of nitric acid (HNO_3) and hydrogen fluoride [HF; 1:1 (v/v)] to remove the native oxide film, followed by distilled water rinse. A platinum foil acted as the cathode electrode. The anodized area was 12 mm × 3 mm and the anodization voltage was fixed at 120 V for different durations. After anodization, the samples were thoroughly washed with distilled water and then dried with air stream. All the experiments were conducted at room temperature. The morphologies of the anodized specimens were characterized by ultra-high-resolution field emission microscope (UHR SEM; FEI XL30), and the cross-section images and the bottom-side images of TiO_2 nanotube arrays were taken from mechanically scratched samples. All the tests were repeated for three times. The results were shown as an average.

Results

Morphology evolution of Ti anodic oxide films

*Figure 1* shows the evolution of surface morphology of
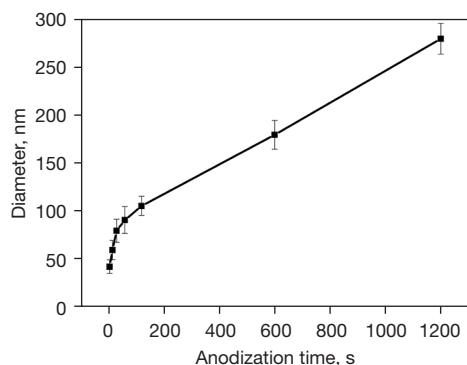
Figure 2 Variation trend of nanohole diameter with time at the initial stage of anodic oxidation.

Ti anodic oxide films obtained at different oxide times when the voltage was 120 V. Nanoholes with diameter of about 40 nm appeared on the surface of anodic oxide film anodized for 5 seconds (*Figure 1A*). When the anodization time was 15 seconds, the diameter of nanoholes increases to about 60 nm (*Figure 1B*). For the oxide film anodized for 2 minutes, the diameter of nanoholes reaches 108 nm (*Figure 1C*). The diameter of nanoholes increases to 180 nm when the anodization time was prolonged to 10 minutes (*Figure 1D*). After 20 minutes of anodization, an obvious nanotube structure was obtained and the diameter of nanotube was almost 280 nm (*Figure 1E*). The nanohole only appeared on the surface of Ti anodic oxide film during the initial stage of anodization, consistent with results reported by other researchers (35). The variation trend of the nanohole diameter with respect to anodization time during the initial stage is illustrated in *Figure 2*. The diameter of the nanoholes increased gradually as the anodization extends, and the rate of diameter growth within the first 2 minutes was greater than in the later phase.

A sequence of scanning electron microscope (SEM) cross-sectional views of the anodic films anodized at 120 V for different durations are shown in *Figure 3*. An approximately compact film, except for some small pits on the surface observed in *Figure 2*, with a length of 200 nm, was obtained when the anodization time was 5 seconds (*Figure 3A*). The oxide film anodized for 15 seconds had a length of 450 nm, and the bottom of this film became an individual hemisphere-like structure, as presented in *Figure 3B*. Meanwhile, it was observed that nanoholes with a length of near 240 nm penetrated into the oxide film, which meant that the whole oxide film contained the upper nanoholes structure and the lower compact film with a thickness

of 190 nm, as shown in *Figure 3C*. The thickness of the lower compact film obtained by anodization for 15 seconds approximated the thickness of the oxide film anodized for 5 seconds. In addition, the nanohole wall exhibited a loomed double-wall interface, indicated by the white line drawn in the lower left inset in *Figure 3C*. We speculate that the oxide film formed at 5 seconds actually contained 2 layers without a clear interface, and the 2-layer structure was hardly detected by SEM. When the anodization time reached 30 seconds, the thickness of oxide film was nearly 780 nm, and the nanohole arrays structure had formed, which should be called nanohole arrays due to the apparent, but not separated boundaries between nanoholes. The wall of some nanoholes had an angular shape (*Figure 3D*). When the anodization time was extended to 2 minutes (*Figure 3E*), the thickness of oxide film was 1,400 nm, and remarkably, the wall division between nanoholes from top to bottom was obvious, indicating the formation of individual nanotubes. The nanotube arrays grew continually and the length reached 3.6 mm when the oxide time was 10 minutes (*Figure 3F*). When the oxidization continued to 20 minutes, the length of nanotube arrays increased to 6 μm (*Figure 3G*). *Figure 4* shows the change trend of thickness of anodic oxide films at the beginning of anodization. Obviously, the rate of thickness growth during the initial 1 minute was significantly higher than during the latter stage. Our experimental results revealed that the growth rate of films was affected by the change of current density, as depicted in *Figure 5*.

The growth rate (R) was represented by the formula: $R = h/t$, where h denotes the thickness of anodic oxide films, measured by SEM cross-section images, as shown in *Figure 3*, and t represents the anodization time. We supposed that the growth of anodic oxide film dominated and the dissolution of anodic oxide film could be ignored temporarily at the initial stage. During the first 5 seconds, the growth rate of anodic oxide film was up to 42 nm/s. Then, the growth rate dropped rapidly to 23 nm/s when the oxidation time was 15 seconds. Subsequently, the growth rate rose to 30.5 nm/s when the anodization time reached 30 seconds, and then the growth rate jumped down again to 18 nm/s at 1 minute. The growth rate diminished continually to 6 nm/s when the anodization lasted for 10 minutes, and further declined to 5.1 nm/s at 20 minutes. Overall, the change trend of the growth rate at the beginning stage of anodization was decreasing dramatically firstly and then increasing slightly, and falling down again more slowly, and finally entering a stable stage, which is analogous to the
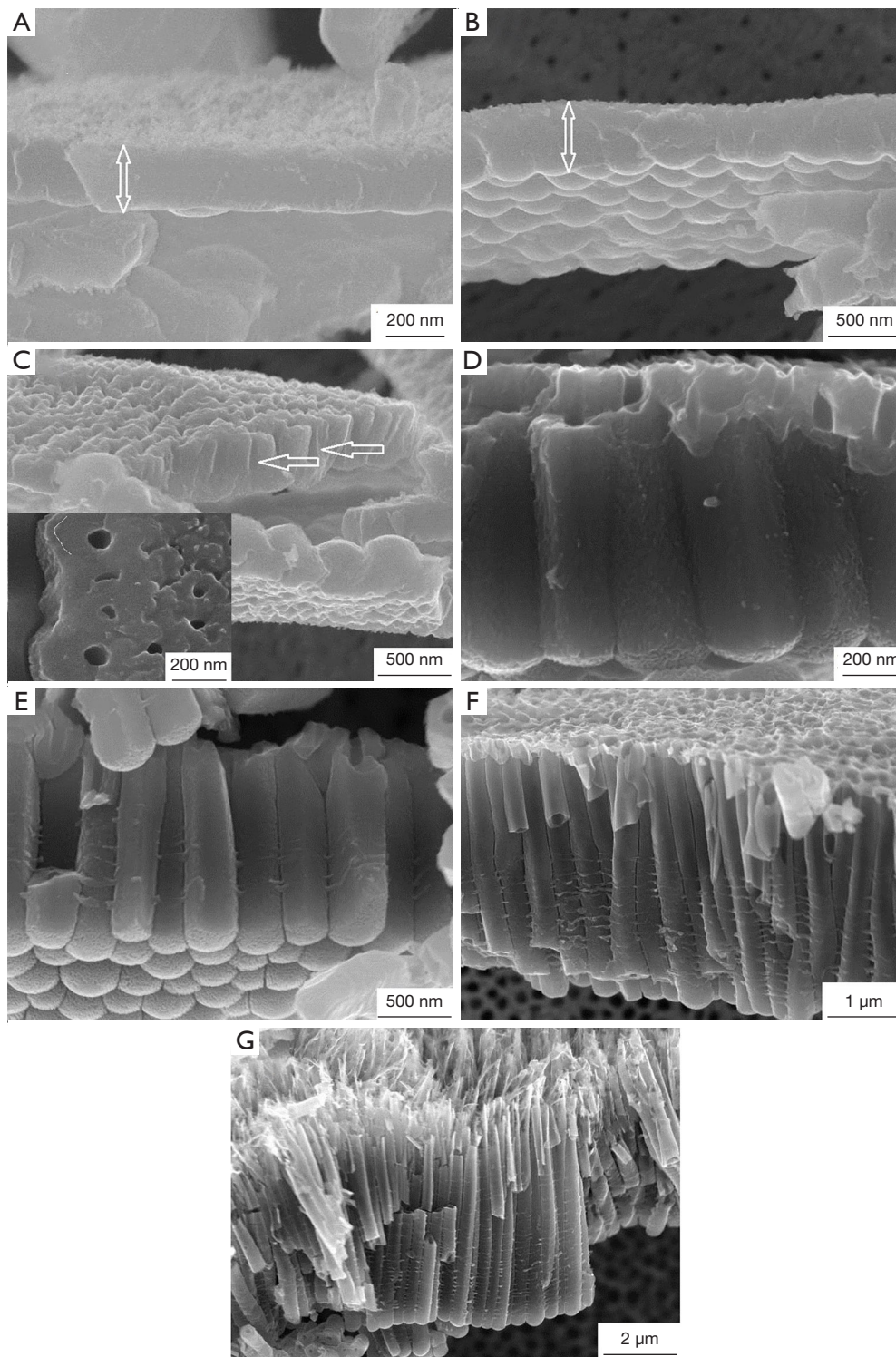
Figure 3 Cross-sectional view of the films anodized at 120 V for different anodic treatment times. (A-G) Anodization for 5 seconds, 15 seconds, 15 seconds, 30 seconds, 2 minutes, 10 minutes and 20 minutes, respectively. The arrows in (A,B) indicate film thickness boundaries, and those in (C) point to the nanohole structure.

Page 6 of 13

Ke et al. Artificial control of the TiO$_2$ nanotube microstructure
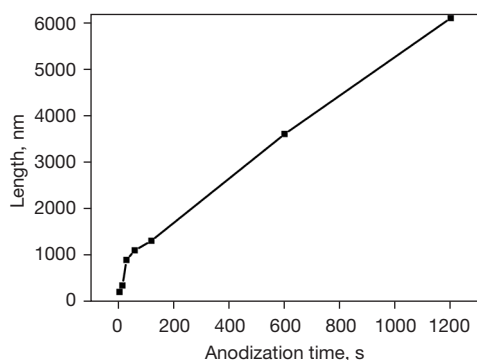
Figure 4 Variation trend of anodic oxide film thickness with time at the initial stage of anodic oxidation.
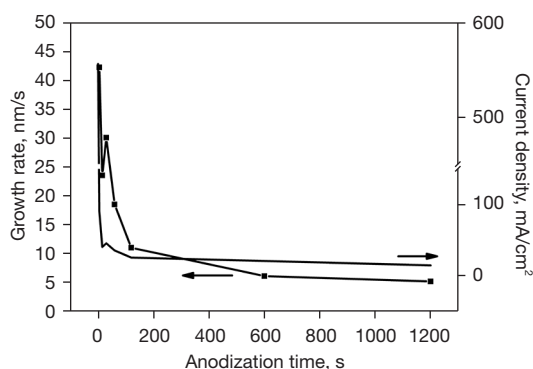
Figure 5 Effect of current density on film growth rate at different anodization time during the initial stage.

change trend with respect to the current density, as shown in *Figure 5*. Although the current density drops sharply at the very beginning of anodization, the current density at this time is still highest during the whole process of anodization, which leads to the highest growth rate at the initial stage. Therefore, we believe that the growth rate of anodic oxide film changes as the current density varies.

Transition from nanoholes to nanotubes

Figure 6 shows the transition process from nanohole to nanotube structure of the anodic oxide film at the initial stage of anodization, that is, the division process of the common wall between nanoholes. As shown in *Figure 6A*, the bottom individual hemisphere-like structure had formed at 30 seconds and the boundaries between individual hemispheres were clear but connected. The shape of the inner holes was close to round and the common walls of

the nanoholes were polygonal and connected, although the boundaries of common walls were visible, as indicated by the white arrows in *Figure 6B*. The double-wall structure of the nanoholes was discernible (upper right inset in *Figure 6B*). It was obvious that anodization for 30 seconds gives birth to the structure of nanohole arrays, even if just irregular nanoholes appear on the surface of the oxide film. When the anodization time was 1 minute, the division between partial hemispheres was visible, as illustrated by the white arrows in *Figure 6C*, and the remaining boundaries between individual hemispheres were connected. *Figure 6D* shows some common walls of nanoholes splitting into individual nanotubular walls, and *Figure 6E* exhibits the incomplete division of common walls, which implies that the nanohole structure begins to transform into a nanotube structure at this stage. As the division of common walls proceeded, the nanohole arrays finally grew to be the nanotube arrays, as shown in *Figure 3E*.

Morphology evolution of remaining Ti substrates

Figure 7 exhibits that the surface morphologies of the remaining Ti substrates after the oxide films, which were anodized at 120 V for different anodization durations, got peeled off. Irregularly and unevenly distributed shallow dimples, which corresponded to the bulge of the bottom individual hemispheres of anodic oxide films, appeared on the remaining Ti substrates after anodization for 5 seconds (*Figure 7A*), even if the individual hemispheres had not been observed by SEM in *Figure 3A* due to slight bulge. After 15 seconds of anodization, the dimples became more apparent and were still irregular (*Figure 7B*), which corresponded to the bulge of the bottom individual hemispheres of anodic oxide film shown in *Figure 3B*. As observed in *Figure 7C*, these dimples obtained at 30 seconds became more regular, and most of them were hexagonal. Meanwhile, the wall of each individual nanohole was polygonal rather than cylindrical. After 1 minute of anodization, the polygon dimples on the remaining Ti substrates were prone to becoming curved (*Figure 7D*), which also showed that the polygonal wall of nanoholes was simultaneously transforming into curved wall of nanotubes.

Discussion

Based on the observations and analysis above, the growth model of large-diameter double-wall TiO$_2$ nanotubes obtained at high voltage is shown in *Figure 8*. In our
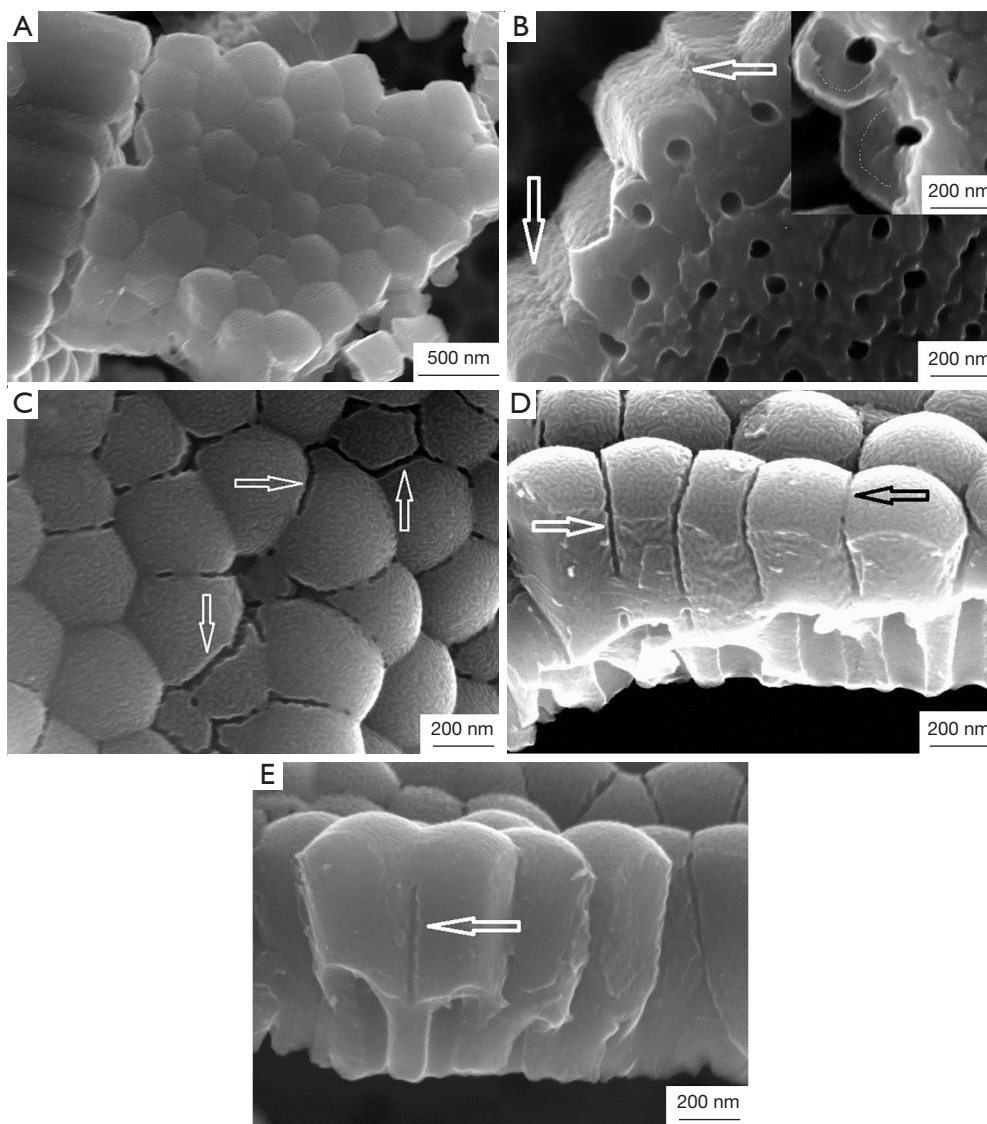
Figure 6 The transition from nanohole structure to nanotube structure of anodic oxide film at the initial stage of anodic oxidation. (A,B) Anodization time: 30 seconds, (C-E) anodization time: 1 minute. Arrows in (B-E) shows boundaries of common walls, the division between partial hemispheres, individual nanotubular walls and incomplete division of common walls, respectively.

experiments, a compact film observed by SEM formed on the titanium substrate at the onset of the anodization as the current density dropped drastically. This phenomenon has been observed in a previous study (36). We infer that the compact film actually contains 2 layers (illustrated in *Figure 8A*): an outer layer (close to the electrolyte) and an inner layer (close to the substrate), even if the delamination is not evident. According to the results reported by Albu *et al.* (31), the carbon species from the electrolyte are mainly incorporated in the inner wall of the tube, and we believe that, although no visible interface exists, the distinction of these 2 layers depends on composition, explicitly, the outer layer exposed to the electrolyte contains, apart from TiO_2, an amount of C and F elements derived from the electrolyte, which is caused by ions migration under strong electrical field (31,34); the inner layer predominantly contains TiO_2 and a small amount of extraneous ions. Carbon species, O^{2-} and F^- migrate from the electrolyte towards the anodic oxide film bottom, and Ti^{4+} migrates from the Ti substrate to the electrolyte as induced by the electric field,

Page 8 of 13

Ke et al. Artificial control of the TiO$_2$ nanotube microstructure
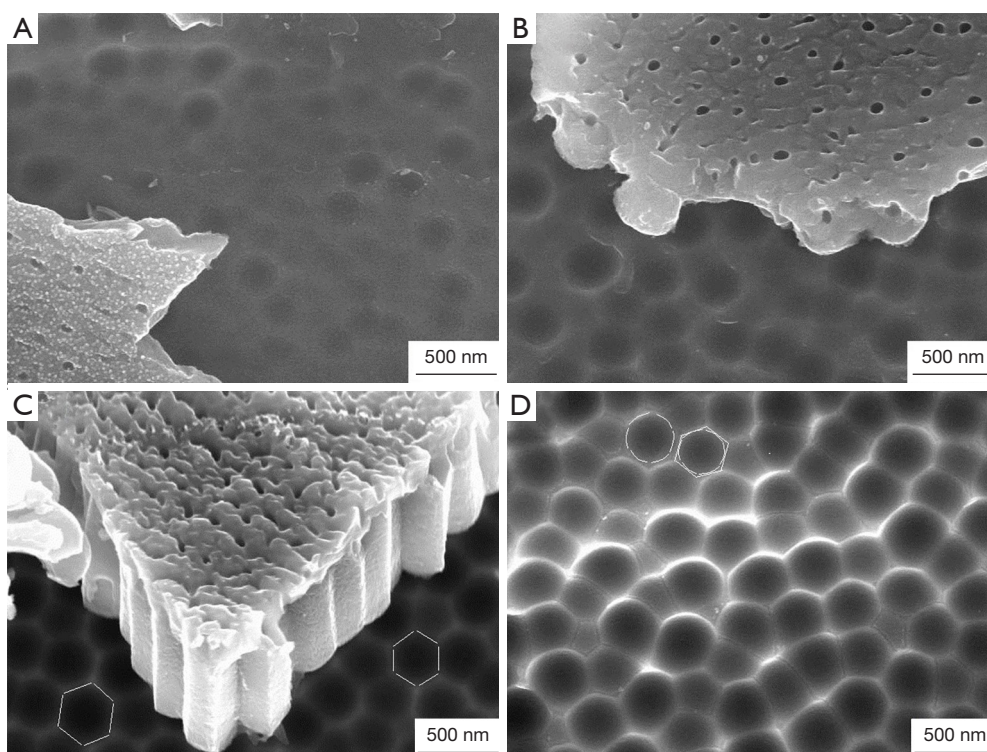

Figure 7 The surface morphology of the remaining Ti substrate after oxidation film stripping at different anode time and 120 V. (A-D) Indicates anodization for 5 seconds, 15 seconds, 30 seconds and 1 minute, respectively.

as illustrated in *Figure 8A*. O^{2-} migrated to the bottom of inner layer react with Ti^{4+} to form continually new compact TiO$_2$ film (37). At the oxide/substrate interface, the growth of compact TiO$_2$ film dominates. According to the insets in *Figure 3C* and *Figure 6B*, we consider that the outer layer is thinner than the inner layer, as drawn in *Figure 8A*.

Subsequently, nanometer-sized shallow pits appeared unevenly on the surface of the compact anodic oxide film (*Figure 8B*), owing to F$^-$ etching the surface of the compact TiO$_2$ film to form soluble [TiF6]$^{2-}$ (37,38). As their diameters increase gradually, the pits also penetrate the compact anodic oxide films, and their depths increase gradually as a result of continual F$^-$ etching. Meanwhile, both flat interfaces at the inner layer bottom and outer layer bottom begin to bulge to form the individual hemisphere-like structure presented above (*Figure 8B*), due to the compressive stress triggered by the volume expansion and electrostrictive forces during the transformation of Ti to TiO$_2$ (18,39), and strong anion adsorption with O^{2-} entrance at the growing oxide lattice (22). Compact TiO$_2$ in the inner layer flows up along the direction indicated by the line with 2 arrows in *Figure 8*, according to the

plastic flow mechanism proposed by Hebert and Houser (22,30), and the outer layer likewise. Under the strong electric field, carbon species, O$_2$, and F$^-$ from electrolyte and Ti^{4+} from Ti substrate keep migrating towards their respective directions. Since the diameter of F$^-$ is less than O^{2-}, the migration speed of F$^-$ is twice as fast as the O^{2-} (40). A fluoride-rich layer consequently forms at the interface between TiO$_2$ anodic oxide film bottom and the remaining Ti substrate (31,37) (dashed bold line in *Figure 8B*). Compact TiO$_2$ forms continuously at the film bottom until the remaining Ti substrate is consumed completely. Carbon species coming from ethylene glycol oxidation products (34) are incorporated into outer layer in form of anions by the electrical field. It is evident that carbon species in the form of anions have a diameter larger than O^{2-} and F$^-$, and we infer that the carbon species cannot pass through the whole oxide film like O^{2-} and F$^-$, and can only permeate the upper part of the oxide film, so the thickness of outer layer is determined by the permeation depth of carbon species related with the applied voltage.

As the etching of F$^-$ towards pits continues, the length of pits increases gradually. Under the push of the plastic flow
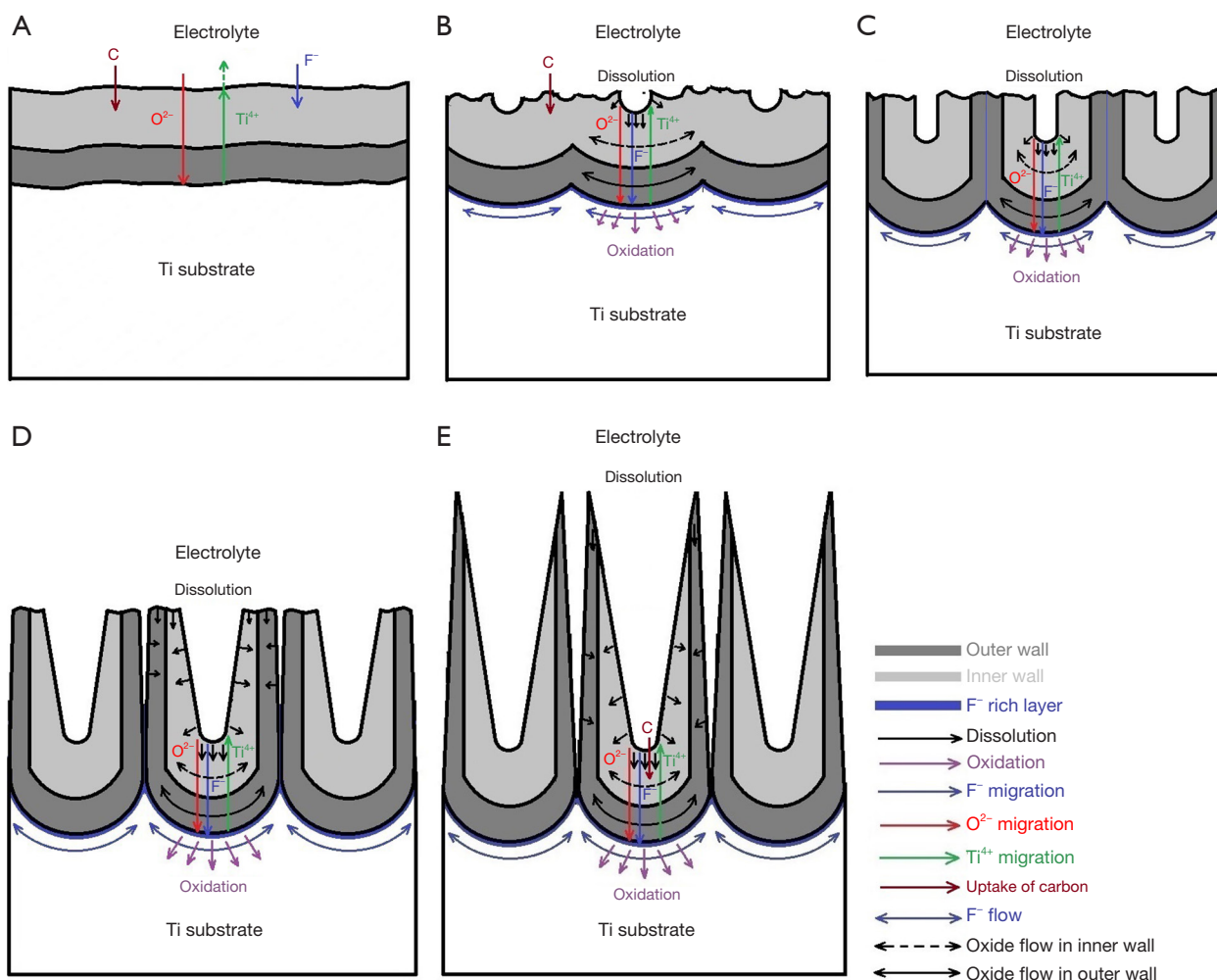
Figure 8 Representation of the formation of the large-diameter and double-walled TiO_2 nanotubes anodized at high voltage: (A) formation of barrier layer; (B) formation of etching pores; (C) nanohole arrays; (D) nanotube arrays; (E) stable growth.

mechanism (18,22), both layers flow up continuously along the directions pointed by 2 arrows in *Figure 8*. Ultimately, inner layer wraps the outer layer to form the initial nanohole wall, namely, a common wall. In this circumstance, the inner layer converts into an outer wall, and the outer layer becomes the inner wall, thus double-wall nanohole arrays form. Meanwhile, the fluoride-rich layer adjacent to the inner layer also moves upward as the inner layer flows up and finally lies in the middle of common walls, as shown in *Figure 8C*. From the inserts in *Figure 3C* and *Figure 6B*, it is apparent that the thickness of the inner wall is far more than that of outer wall with a ratio of about 3:2. Moreover, we also found that the ratio of inner wall to outer wall at the bottom of the TiO_2 nanotube anodized by different high voltages (120–225 V) in our experiments is also ~2–3. Also,

at this stage, carbon species, O^{2-}, F^-, and Ti^{4+} also migrate towards respective directions, and new compact TiO_2 keeps growing at the bottom of the anodic oxide film and the top of oxide film keeps dissolving because of the electrolyte etching.

Since the fluoride-rich layer exists in the middle of common walls of nanohole arrays, the dissolution of fluoride-rich layer into the electrolyte results in the division of the common wall of TiO_2 nanohole array (41), which means that the TiO_2 nanotube arrays forms (*Figure 8D*). The outer and inner walls of nanoholes are polygonal, and the polygonal outer and inner nanohole walls gradually become the curved outer and inner walls after the common nanohole walls separate. Except for the etching from electrolyte, we suggest that instinctive contraction force

Page 10 of 13

Ke et al. Artificial control of the TiO₂ nanotube microstructure
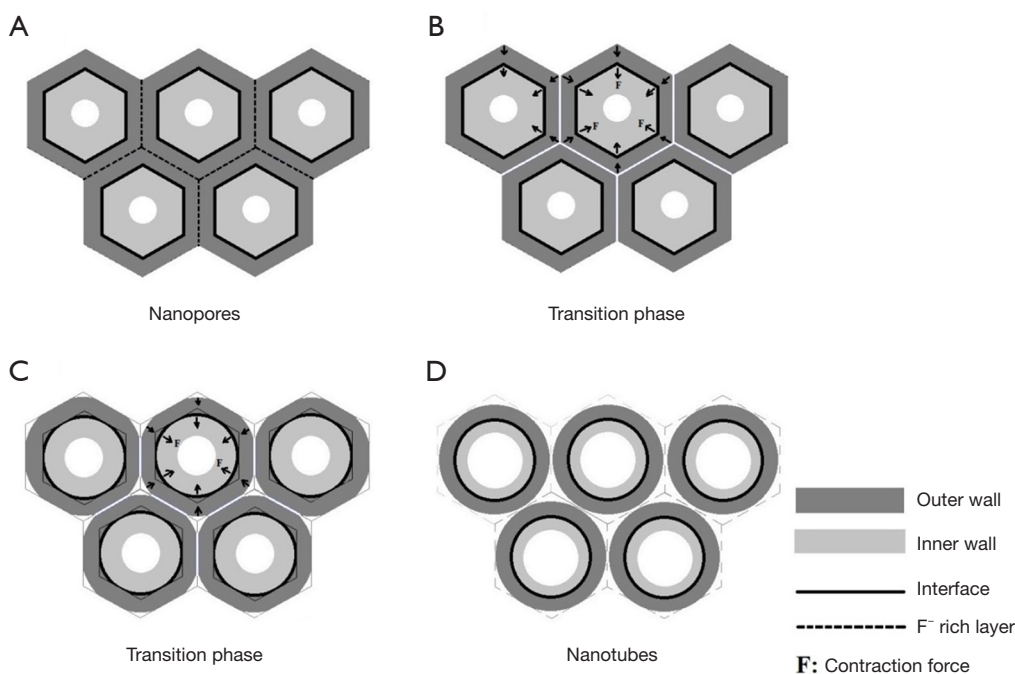
Figure 9 Transformation from polygonal structure of double-walled nanohole arrays to approximately cylindrical structure of double-walled nanotube arrays: (A) nanopores; (B) transition phase; (C) transition phase; (D) nanotubes.

from the self-regulation mechanism of TiO₂ nanotubes, perhaps caused by the material plastic flow, also makes the polygonal inner and outer nanohole walls become cylindrical. Based on the speculation above, the transition from the polygonal structure of double-wall nanohole array to the approximately cylindrical structure of double-wall nanotube arrays is shown in *Figure 9*; we also speculate the ideal regular hexagonal nanohole in *Figure 9*. Certainly, the shape of nanoholes is polygonal, including an irregular pentagon and hexagonal in our experiments. As the whole surface of the inner walls is always exposed to the electrolyte during anodization, a large amount of carbon species are incorporated into the inner wall (34), which leads to higher dissolution rate of the inner wall in electrolyte than the outer wall (33). In our previous works (33), it was reported that the inner wall/outer wall interface of the TiO₂ nanotube anodized at higher than 120 V had an obviously porous structure, and the interface anodized at lower than 120 V was hardly detected by SEM (33). We infer that it is possibly caused by the different plastic flow speed and different instinctive contraction force, both resulting from different composition of inner wall and outer wall. For TiO₂ nanotubes obtained at lower than 120 V, owing to the lower applied voltage, the film is thinner, and the amount of

impurity is comparably low, leading to the interaction force between inner wall and outer wall weakening. This explains why the porous interface is not obvious. Here, the tube top wall becomes even thinner and the compact TiO₂ grows continuously at the bottom.

Along with the growth of the tube bottom and the dissolution of the tube top, the length of nanotubes increases gradually, and the tube top becomes thinner due to the etching from electrolyte, and eventually V-shaped large-diameter double-wall TiO₂ nanotube forms, as depicted in *Figure 8E*.

In recent years, researchers have been optimizing and developing the anodic oxidation method, breaking away from the traditional one-step anodic oxidation method, and gradually mainstream the two-step anodic oxidation method (42), suggesting further directions for this study.

Conclusions

In this manuscript, the growth process of large-diameter double-wall TiO₂ nanotubes fabricated by anodization at 120 V on pure titanium foil in ethylene glycol electrolyte consisting of NH₄F and H₂O was investigated. Based on our observations and inspirations garnered from existing

literatures, the growth models corresponding to different growth stages were established and then a detailed discussion of the growth mechanism was presented. The following conclusions can be drawn:

(I) At the initial stage of anodization, only nanoholes appear on the surface of anodic oxide films, and the diameter of nanoholes increase gradually with the anodization time. An approximately compact film forms after 5 seconds of anodization, and an obvious bottom individual hemisphere-like structure appears at 15 seconds. The growth rate of anodic oxide film changes accordingly with the current density, which means the former is affected by the latter.

(II) When the anodization time is 1 minute, partial nanoholes begin to split into nanotubes. Meanwhile, the polygonal wall of nanotubes begins to become curved. The dimples, which were irregularly polygonal and unevenly distributed on the surface of the remaining Ti substrate, become regularly round and evenly distributed.

(III) According to the growth models corresponding to different growth stages, we consider the compact anodic oxide film formed initially actually contains outer layer and inner layer, with no obvious interface between them. The bottom even levels of the inner layer and outer layer bulge towards the substrate and become individual hemisphere-like structures under the action of compress stresses and the plastic flow mechanism. The inner layer becomes the outer wall, and the outer layer becomes inner wall. Instinctive contraction force possibly leads to polygonal inner and outer walls becoming cylindrical except for the etching of electrolyte. Instinctive contraction force and different plastic flow speed are probably the cause of the porous inner wall/outer wall interface. Eventually, V-shaped large-diameter and double-wall TiO_2 nanotube arrays form.

Acknowledgments

Footnote

Reporting Checklist: The authors have completed the MDAR reporting checklist. Available at https://atm.amegroups.com/article/view/10.21037/atm-22-6510/rc

Data Sharing Statement: Available at https://atm.amegroups.com/article/view/10.21037/atm-22-6510/dss

Conflicts of Interest: All authors have completed the ICMJE uniform disclosure form (available at https://atm.amegroups.com/article/view/10.21037/atm-22-6510/coif). All authors report funding support from the National Natural Science Foundation of China (Nos. 51401126, 81401819); Zhejiang Provincial Natural Science Foundation of China (Nos. BY22H181190, LGF21H060003); "Science and Technology Innovation 2025" Major Special Project of Ningbo (No. 2019B10064); and Ningbo Natural Science Foundation (Nos. 2018A610203, 202002N3195, 202002N3125). JN is from Ningbo Regen Biotech, Co., Ltd. The authors have no other conflicts of interest to declare.

Ethical Statement: The authors are accountable for all aspects of the work in ensuring that questions related to the accuracy or integrity of any part of the work are appropriately investigated and resolved.

References

1. Li G, Liu ZQ, Zhang Z, et al. Preparation of Titania Nanotube Arrays by the Hydrothermal Method. Chinese Journal of Catalysis 2009;30:37-42.
2. Jung JH, Kobayashi H, Bommel K, et al. Creation of novel helical ribbon and double-layered nanotube TiO2 structures using an organogel template. Chemistry of

Page 12 of 13

Ke et al. Artificial control of the TiO₂ nanotube microstructure

Materials 2002;14:1445-7.

3. Feng E, Shen K, Lin F, et al. Improved osteogenic activity and inhibited bacterial biofilm formation on andrographolide-loaded titania nanotubes. Ann Transl Med 2020;8:987.

4. Ocampo RA, Echeverria FE. Antibacterial and Biological Behavior of TiO2 Nanotubes Produced by Anodizing Technique. Crit Rev Biomed Eng 2021;49:51-65.

5. Park J, Cimpean A, Tesler AB, et al. Anodic TiO(2) Nanotubes: Tailoring Osteoinduction via Drug Delivery. Nanomaterials (Basel) 2021;11:2359.

6. Gultepe E, Nagesha D, Sridhar S, et al. Nanoporous inorganic membranes or coatings for sustained drug delivery in implantable devices. Adv Drug Deliv Rev 2010;62:305-15.

7. Popat KC, Eltgroth M, Latempa TJ, et al. Decreased Staphylococcus epidermis adhesion and increased osteoblast functionality on antibiotic-loaded titania nanotubes. Biomaterials 2007;28:4880-8.

8. Kodama A, Bauer S, Komatsu A, et al. Bioactivation of titanium surfaces using coatings of TiO(2) nanotubes rapidly pre-loaded with synthetic hydroxyapatite. Acta Biomater 2009;5:2322-30.

9. Tsuchiya H, Macak JM, Müller L, et al. Hydroxyapatite growth on anodic TiO2 nanotubes. J Biomed Mater Res A 2006;77:534-41.

10. Mor GK, Shankar K, Paulose M, et al. Use of highly-ordered TiO(2) nanotube arrays in dye-sensitized solar cells. Nano Lett 2006;6:215-8.

11. Zhu K, Neale NR, Miedaner A, et al. Enhanced charge-collection efficiencies and light scattering in dye-sensitized solar cells using oriented TiO2 nanotubes arrays. Nano Lett 2007;7:69-74.

12. Paramasivam I, Macak JM, Schmuki P. Photocatalytic activity of TiO2 nanotube layers loaded with Ag and Au nanoparticles. Electrochemistry Communications 2008;10:71-5.

13. Macak JM, Schmidt-Stein F, Schmuki P. Efficient oxygen reduction on layers of ordered TiO2 nanotubes loaded with Au nanoparticles. Electrochemistry Communications 2007;9:1783-7.

14. Hahn R, Ghicov A, Tsuchiya H, et al. Lithium-ion insertion in anodic TiO2 nanotubes resulting in high electrochromic contrast. physica status solidi (a) 2007;204:1281-5.

15. Brammer KS, Oh S, Cobb CJ, et al. Improved bone-forming functionality on diameter-controlled TiO(2) nanotube surface. Acta Biomater 2009;5:3215-23.

16. Albu SP, Ghicov A, Macak JM, et al. Self-organized, free-standing TiO2 nanotube membrane for flow-through photocatalytic applications. Nano Lett 2007;7:1286-9.

17. Ghicov A, Schmuki P. Self-ordering electrochemistry: a review on growth and functionality of TiO2 nanotubes and other self-aligned MO(x) structures. Chem Commun (Camb) 2009;(20):2791-808.

18. Roy P, Berger S, Schmuki P. TiO2 nanotubes: synthesis and applications. Angew Chem Int Ed Engl 2011;50:2904-39.

19. Thompson GE. Porous anodic alumina: fabrication, characterization and applications. Thin Solid Films 1997;297:192-201.

20. Jessensky O, Müller F, Gösele U. Self-organized formation of hexagonal pore arrays in anodic alumina. Applied Physics Letters 1998;72:1173-5.

21. Macdonald DD. On the formation of voids in anodic oxide films on aluminum. Journal of the Electrochemical Society 1993;140:L27-30.

22. Houser JE, Hebert KR. The role of viscous flow of oxide in the growth of self-ordered porous anodic alumina films. Nat Mater 2009;8:415-20.

23. Zwilling V, Darque-Ceretti E, Boutry-Forveille A, et al. Structure and physicochemistry of anodic oxide films on titanium and TA6V alloy. Surface and Interface Analysis 1999;27:629-37.

24. Beranek R, Hildebrand H, Schmuki P. Self-Organized Porous Titanium Oxide Prepared in H[sub 2]SO[sub 4]/HF Electrolytes. Electrochemical and Solid-State Letters 2003;6:B12.

25. Mor GK, Varghese OK, Paulose M, et al. Fabrication of tapered, conical-shaped titania nanotubes. Journal of Materials Research 2003;18:2588-93.

26. Gong D, Grimes CA, Varghese OK, et al. Titanium oxide nanotube arrays prepared by anodic oxidation. Journal of Materials Research 2001;16:3331-4.

27. Choi J, Wehrspohn RB, Lee J, et al. Anodization of nanoimprinted titanium: a comparison with formation of porous alumina. Electrochimica Acta 2004;49:2645-52.

28. Skeldon P, Thompson GE, Garcia-Vergara SJ, et al. A Tracer Study of Porous Anodic Alumina. Electrochemical and Solid-State Letters 2006;9:B47.

29. Garcia-Vergara SJ, Skeldon P, Thompson GE, et al. A flow model of porous anodic film growth on aluminium. Electrochimica Acta 2006;52:681-7.

30. Hebert KR, Houser JE. A Model for Coupled Electrical Migration and Stress-Driven Transport in Anodic Oxide Films. Journal of The Electrochemical Society

2009;156:C275.

31. Albu SP, Ghicov A, Aldabergenova S, et al. Formation of Double-Walled TiO2 Nanotubes and Robust Anatase Membranes. Advanced Materials 2008;20:4135-9.

32. Raja KS, Misra M, Paramguru K. Formation of self-ordered nano-tubular structure of anodic oxide layer on titanium. Electrochimica Acta 2005;51:154-65.

33. Ni J, Noh K, Frandsen CJ, et al. Preparation of near micrometer-sized TiO2 nanotube arrays by high voltage anodization. Mater Sci Eng C Mater Biol Appl 2013;33:259-64.

34. Liu N, Mirabolghasemi H, Lee K, et al. Anodic TiO2 nanotubes: double walled vs. single walled. Faraday Discuss 2013;164:107-16.

35. Yuan X, Zheng M, Ma L, et al. High-speed growth of TiO2 nanotube arrays with gradient pore diameter and ultrathin tube wall under high-field anodization. Nanotechnology 2010;21:405302.

36. Berger S, Kunze J, Schmuki P, et al. A lithographic approach to determine volume expansion factors during anodization: Using the example of initiation and growth of TiO2-nanotubes. Electrochimica Acta 2009;54:5942-8.

37. Macak JM, Tsuchiya H, Ghicov A, et al. TiO2 nanotubes: Self-organized electrochemical formation, properties and applications. Current Opinion in Solid State and Materials Science 2007;11:3-18.

38. Yin H, Liu H, Shen WZ. The large diameter and fast growth of self-organized TiO2 nanotube arrays achieved via electrochemical anodization. Nanotechnology 2010;21:035601.

39. Yasuda K, Macak JM, Berger S, et al. Mechanistic Aspects of the Self-Organization Process for Oxide Nanotube Formation on Valve Metals. Journal of The Electrochemical Society 2007;154:C472.

40. Habazaki H, Fushimi K, Shimizu K, et al. Fast migration of fluoride ions in growing anodic titanium oxide. Electrochemistry Communications 2007;9:1222-7.

41. Berger S, Hahn R, Roy P, et al. Self-organized TiO2 nanotubes: Factors affecting their morphology and properties. physica status solidi (b) 2010;247:2424-35.

42. Fu Y, Mo A. A Review on the Electrochemically Self-organized Titania Nanotube Arrays: Synthesis, Modifications, and Biomedical Applications. Nanoscale Res Lett 2018;13:187.

(English Language Editor: J. Jones)